Controlling Molecular Self-Organization: Formation of Nanometer-Scale Spheres and Tubules

G. William Orr, Leonard J. Barbour, Jerry L. Atwood*

Amphiphilic polyhedron-shaped *p*-sulfonatocalix[4]arene building blocks, which have been previously shown to assemble into bilayers in an antiparallel fashion, have been assembled in a parallel alignment into spherical and helical tubular structures by the addition of pyridine *N*-oxide and lanthanide ions. Crystallographic studies revealed how metal ion coordination and substrate recognition direct the formation of these supramolecular assemblies. The addition of greater amounts of pyridine *N*-oxide changed the curvature of the assembling surface and resulted in the formation of extended tubules.

Supramolecular architectures with spherical and tubular morphologies have potential fundamental and practical implications in areas such as materials science, biomimetic chemistry, and molecular electronics (*1–3*). Important models for the design of artificial systems exhibiting such structural morphologies may be borrowed from biology and include, for example, the spherical and tubular protein coat structures of viruses (*4*) and the helical array of tubulin subunits in microtubule protein fibers (*5*). However, in these macromolecular systems, assembly and structural morphology are highly dependent on the immense size of the protein structural components. Therefore, in the construction of artificial systems bearing these morphologies (*2, 6*), especially when nanometer-scale periodicities are required, there is a need for design strategies that can be applied to small-molecule building blocks.

p-Sulfonatocalix[4]arene^{5-} (**1**, Fig. 1A) is a macrocyclic anion that has a truncated pyramid shape and contains a hydrophobic cavity bounded by four aromatic rings. The base and apical square faces of the truncated pyramid are defined by sulfonate groups and phenolic hydroxyl groups, respectively, and the trapezoidal faces consist of the external surfaces of the aromatic rings. The bipolar amphiphilic nature of **1**, in conjunction with its truncated pyramidal shape, serves as a dominant structure-directing factor in the organization of this macrocycle in its solid-state structures. For example, in the crystal structure (*7*) of Na_5**1**, the hydrophobic cores of the truncated pyramids align to form a bilayered structure consisting of alternating organic and aqueous layers. This structure is consistent with the arrangement of a bipolar amphiphilic molecule according to the influences of hydrophobic effects (*8*). The aqueous layers are composed of the polar surfaces of the truncated pyramids, water molecules, and counterions. The organic layers consist of a π-stacked, two-dimensional bilayered grid composed of truncated pyramids arranged in an alternating "up-down" antiparallel fashion with their aromatic rings in van der Waals contact with those of adjacent calixarene molecules. This aspect of the structure may be interpreted in terms of organization of the truncated pyramids according to shape complementarity (*9*).

Although the bilayer arrangement of **1** persists in many of its structures that we have investigated (*10*), we nonetheless anticipated that it should be possible to influence the relative orientation of the truncated pyramids with respect to each other. Moreover, we sought to "engineer" the orientation of the truncated pyramids into an "up-up" arrangement. We arrived at a design strategy that uses a three-component system consisting of Na_5**1**, pyridine *N*-oxide (**2**), and a lanthanide metal (Ln^{3+}) nitrate (Fig. 1). In a representative example, aqueous solutions of Na_5**1** (0.283 M), **2** (3.07 M), and $La(NO_3)_3 \cdot 6H_2O$ (1.15 M) were combined in a 2:2:1 molar ratio. After ~1 hour, crystals formed that were suitable for single-crystal x-ray diffraction analysis (*11*). The crystal structure reveals a framework in which two *p*-sulfonatocalix[4]arene anions **1** coordinate to a La^{3+} ion through their sulfonate groups to form a C-shaped dimeric assembly (Fig. 1H). In addition, two pyridine *N*-oxide ligands, both of which coordinate to the La^{3+} ion, are bound within the respective calixarene cavities of the dimer. In these dimeric assemblies, the Ln^{3+} ion acts as a hinge, and the steric requirements of the pyridine *N*-oxide ligands binding concomitantly to the Ln^{3+} ion and the calixarene cavities, impart a dihedral angle of ~60° between the *p*-sulfonatocalix[4]arene molecules.

This structural feature helps **1** assemble into structures with curved surfaces, such as spherical clusters (**3**, Figs. 1, A through C, and 2) composed of 12 *p*-sulfonatocalix[4]arene molecules arranged at the vertices of an icosahedron. These spherical assemblies measure ~28 Å (2.8 nm) in diameter and have a volume of ~11,000 $Å^3$ (11 nm^3). As in the bilayer structures observed for Na_5**1**, the hydrophobic regions of the truncated pyramid-shaped anions are aligned, but in this case, they are assembled in an "up-up" radially symmetric fashion along the surface of a sphere, where they constitute an organic shell around an aqueous polar core (Figs. 1C and 2). Thus, 48 negatively charged sulfonate groups from the larger faces of 12 truncated pyramids lie on the exterior of the sphere and define a polar outer shell surface (Fig. 2A). Similarly, a polar inner shell surface comprises 48 phenolic hydroxyl groups, 12 of which are deprotonated, from the smaller faces of the truncated pyramids. This arrangement is consistent with that often observed in unilamellar vesicles in which the larger polar head groups of bipolar amphiphiles are preferentially oriented toward the external surface of the membrane, and the smaller polar head groups are oriented toward the interior (*12*).

The cavities of the calixarenes in **3** lie just below the polar surface of the sphere and constitute a series of hydrophobic pockets. Twelve pyridine *N*-oxide molecules penetrate the polar surface of each sphere and bind within the hydrophobic pockets through π-stacking interactions, and their O atoms extend outward from the pockets and coordinate to La^{3+} ions above the sphere surface. The aqueous interstitial areas between spheres contain, in addition to La^{3+} ions, an intricate H-bonded network of water molecules and hydrated Na^+ ions. The core of each sphere has a diameter of ~15 Å and a volume of ~1700 $Å^3$ and contains a well-defined cluster consisting of 30 water molecules and two Na^+ ions. This cluster plays an important role in stabilizing the supramolecular structure of the spherical assembly (*13*) (Fig. 2B). The Na^+ ions and 12 water molecules form a H-bonded $[Na(H_2O)_6]_2$ dimer in which the Na^+ ions reside at opposite vertices of a cube, and the O atoms of a cyclic hexameric H-bonded array of water molecules supply the other six corners of the cube. The remaining water molecules form a sheath that surrounds the $[Na(H_2O)_6]_2$ dimer and links it to the polar inner shell surface through H-bonding interactions (*14*).

When aqueous solutions of Na_5**1** (0.283 M), **2** (3.07 M), and $La(NO_3)_3 \cdot 6H_2O$ (1.15 M) were combined in a 2:8:1 molar ratio, needle-shaped crystals formed after several days. Crystallographic analysis (*15*) of these crystals reveals a tubular assembly (**4**, Figs. 1 and 3) ~28 Å (2.8 nm) in diameter and consisting of *p*-sulfonatocalix[4]arene molecules

---

Department of Chemistry, University of Missouri–Columbia, Columbia, MO 65211, USA.

*To whom correspondence should be addressed. E-mail: AtwoodJ@missouri.edu

arranged along the surface of a cylinder. The tubes are aligned with the long axis of the needle-shaped crystals and therefore have lengths approaching 1 cm in some cases. A cross-sectional view (Fig. 1E) of the tubular assembly bears a close resemblance to that of 3 (Fig. 1C) and consists of an analogous polar core, an organic shell, and a polar inner and outer shell surface. As in 3, the sulfonate groups of the truncated pyramid-shaped calixarenes comprise a polar outer surface, and the hydroxyl groups define a polar inner shell surface. In 4, however, the organic shell is no longer purely composed of calixarene molecules but contains two crystallographically unique pyridine *N*-oxide molecules intercalated between the aromatic rings of adjacent calixarenes (Fig. 3A). One type is disordered and is oriented such that its O atom is directed toward the interior of the tube (Fig. 3B). The other type is oriented such that its O atom is directed toward the outer polar surface of the tube where it coordinates to Na^+ ions (Fig. 1F). In addition, each participates in π-stacking interactions (*16*) (both T-shaped and parallel-offset types) with the aromatic rings of four surrounding calixarene molecules (Fig. 3A).

Another notable feature of **4** is that the *p*-sulfonatocalix[4]arene molecules and the intercalated pyridine *N*-oxide molecules form a chiral helical assembly along the length of the tube (Fig. 3, A and B). The helix consists

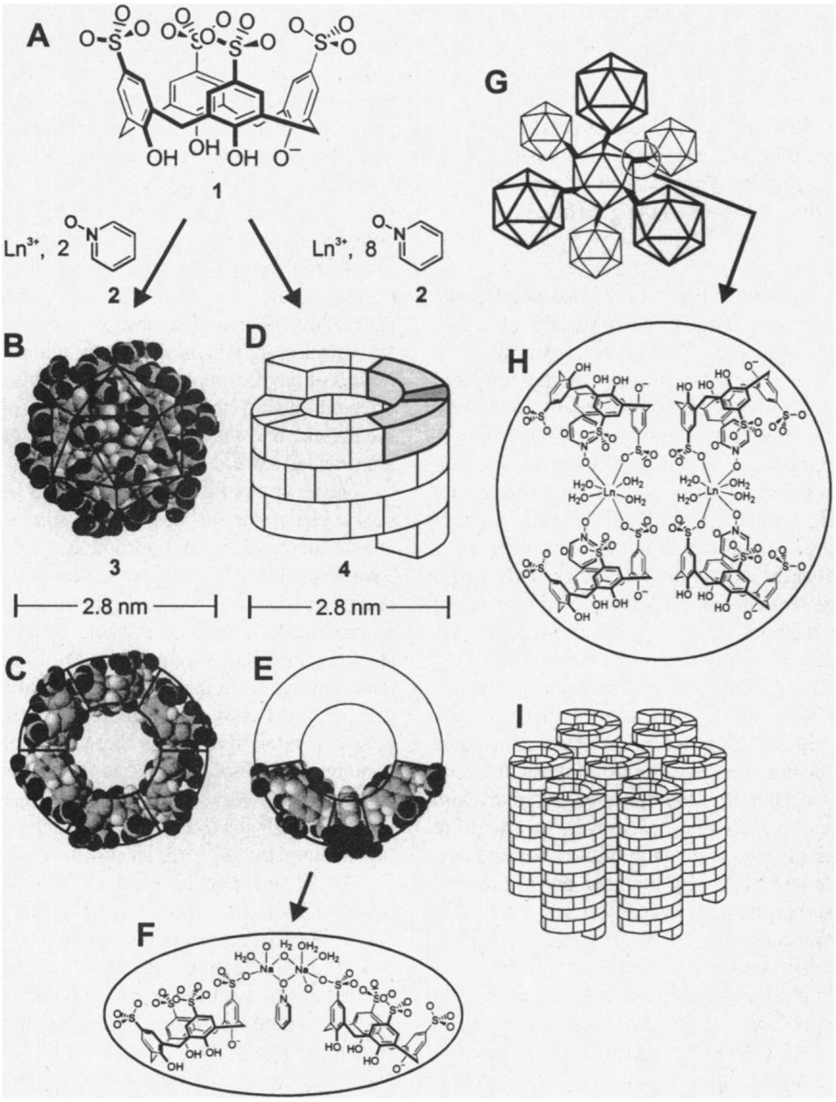

Fig. 1. Schematic representation of the self-organization of (**A**) *p*-sulfonatocalix[4]arene anions **1** into structures with spherical **3** (A through C) and tubular **4** (D through F) morphologies and higher aggregates (G and I). (**B**) In the presence of **2** and Ln^{3+} (in a 2:2:1 molar ratio), spherical supermolecules **3** form that contain 12 *p*-sulfonatocalix[4]arene anions. In **3**, the centroid of a *p*-sulfonatocalix[4]arene anion lies at each vertex of the icosahedron (actual crystallographic coordinates shown). (**C**) Cross-sectional view of **3** illustrating the "up-up," shape-complementary arrangement of the truncated pyramid-shaped anions **1** (outlined) to form a curved surface. Adjacent calixarenes are linked by π-stacking interactions. (**D**) Tubular assemblies **4** form at molar ratios of 2:8:1 of **1**, **2**, and Ln^{3+}. The tubes are composed of **1** and **2** (shaded) alternating around the surface of a cylinder in a chiral helical fashion. There are 4.5 units of **1** and **2** per turn of the helix. (**E**) Partial cross-sectional view of **4** showing the π-stacked, shape-complementary arrangement of **1** and **2** (outlined), forming the curved surface that defines the tube. (**F**) In the tubular assemblies **4**, pyridine *N*-oxide molecules intercalate between the aromatic rings of adjacent anions of **1** through π-stacking interactions. (**G**) Each sphere **3** is connected to six surrounding spheres. (**H**) Linkages between spheres consist of two C-shaped dimers. (**I**) Tubular assemblies **4**, which are also connected by C-shaped dimers similar to those shown in (H), are organized in a hexagonal array.

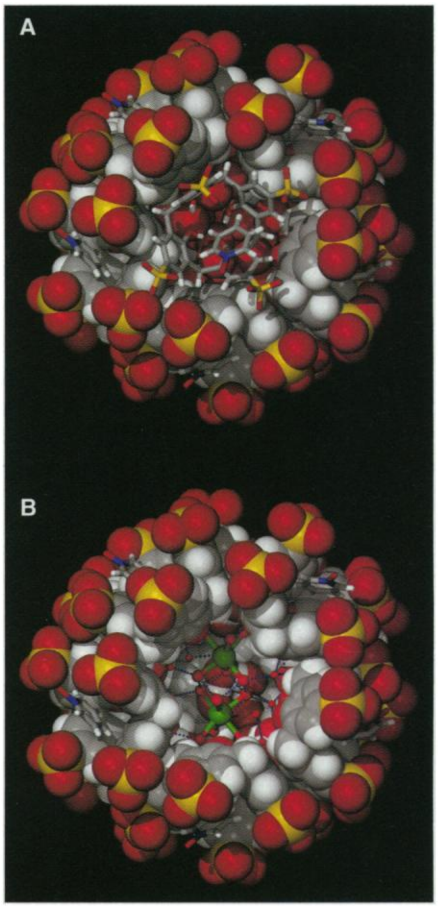

Fig. 2. Structure of the spherical assembly **3**. (**A**) Partial space-fill view along a pseudo-five-fold axis. Pyridine *N*-oxide guest molecules and one *p*-sulfonatocalix[4]arene anion are shown in stick mode. Elements are colored as follows: C, gray; H, white; N, blue; O, red; and S, yellow. Sulfonate groups (SO_3^-) line the polar exterior surface of the sphere; aromatic rings define the hydrophobic shell. The polar core comprises 30 water molecules and two Na^+ ions. (**B**) Cutaway view showing an $[Na(H_2O)_6]_2$ cluster (Na shown in green) within the core of **3**. Hydrogen-bonding contacts are shown as dashed blue lines (H atoms could not be located). Two hexaaquasodium complexes are linked together by six H bonds. Coordinated water molecules H bond to uncoordinated water molecules, which in turn H bond to phenolic O atoms of the polar inner shell surface.

of a single strand of alternating **1** and **2**, and there are 4.5 of these units in each turn (Fig. 1). These tubular assemblies are arranged in a hexagonal array (Fig. 1I) in a pattern similar to the organization of cylindrical micelles (*17*). The Na^+ ions assist in stabilizing the tubular assemblies by coordinating to the sulfonate groups of calixarenes in adjacent turns of the helix. In this structure, there are two types of pyridine *N*-oxide molecules that fill the calixarene cavities. One type is bound within the calixarenes of the C-shaped dimers and is coordinated to La^{3+} ions that, in turn, join adjacent tubes. The second type is disordered, and its O atom extends into a triangular-shaped tunnel that is lined by the outer surfaces of three adjoining tubes. These tunnels, which contain a disordered network of water molecules and Na^+ ions, are created by the hexagonal packing arrangement of the tubes. Here too, the C-shaped dimers persist, but the dihedral angle between the calixarene molecules is only ~15°. In proceeding from the sphere to the tube, the aqueous core has become a cylindrical channel with a diameter of ~15 Å. This channel, which is not well resolved because of disorder, contains La^{3+} ions in addition to the hydrated Na^+ ions observed in the spherical core.

The intercalation of **2** into the organic shell has an effect equivalent to increasing the hydrophobic volume of the structural components that make up the shell but that contribute little to their polarity. According to the concept of critical packing parameters (*12*), which is a model developed to predict the packing shapes of lipid membranes, an increase in the volume of the hydrophobic portion of a given amphiphile, other factors remaining constant, will tend to favor the formation of a cylindrical rather than a spherical structure. This model offers at least a qualitative explanation for the transition from the spherical morphology seen for **3** to the tubular morphology observed in **4**.

The generality of this design strategy was explored with respect to a number of factors. Spherical structures completely analogous to **3** are obtained with other lanthanide ions, including Pr, Nd, Eu, Gd, Tb, Dy, Er, and Yb. Because of the similarity in coordination tendencies through the lanthanide series, this result should perhaps not be surprising. In the case of the tubular structures **4**, a thorough investigation was hampered by the small size and delicate nature of the crystals, but nonetheless, it was possible to obtain an analogous tubular structure for Gd and Yb. Although there are slight differences in unit cell dimensions and in some minor features of the structures, the spherical and tubular calixarene assemblies are essentially identical throughout the series. Therefore, it appears that variations in the size of the lanthanide ions are absorbed by subtle changes in intermolecular bond distances and angles in the surrounding interstitial areas, but the geometry of the spheres and tubes is conserved.

The results presented here exemplify the enormous potential of self-organization toward the construction of solids with well-defined structural morphologies and periodicities on the nanometer scale. In these structures, hydrophobic effects and numerous noncovalent interactions, such as metal-ligand coordination, π-stacking interactions, H bonds, and van der Waals forces, all play roles in the assembly of small-molecule structural components according to size, shape, and polarity. The generality of this noncovalent synthetic approach suggests that a range of structures with different sizes, morphologies, structural components, and (ultimately) functions could be produced with appropriate modifications.

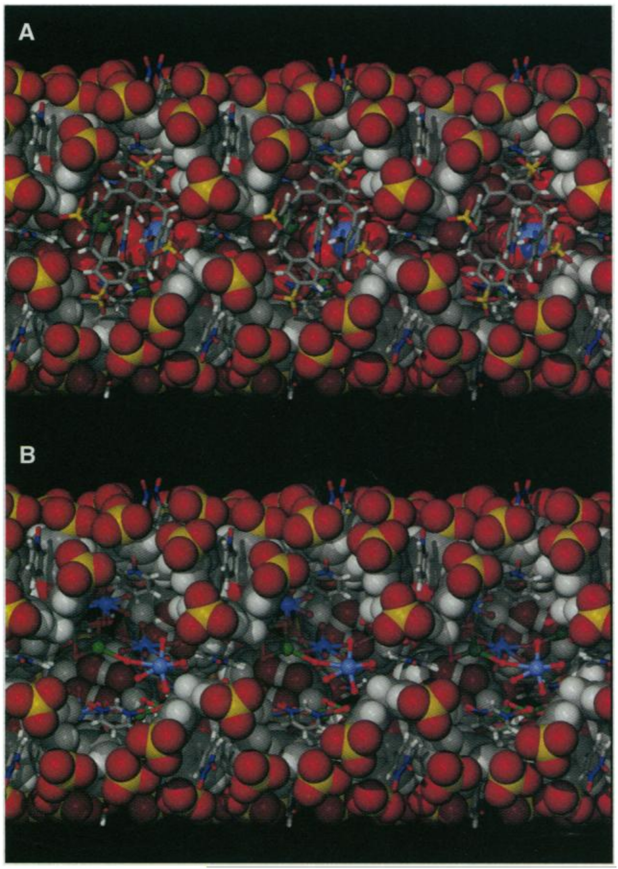

Fig. 3. Structure of the tubular assembly **4**. (**A**) Partial space-fill view perpendicular to the tube showing six turns of the helix. *p*-Sulfonatocalix[4]arene anions shown in stick mode mark two turns of the helix. Pyridine *N*-oxide molecules are shown in stick mode. There are π-stacking interactions between **1** and **2** along the turns of the helix. (**B**) Cutaway view showing the hydrated Na^+ and La^{3+} ions (light blue) within the cylindrical channel.

References and Notes

1. R. H. Vreekamp, J. P. M. van Duynhoven, M. Hubert, W. Verboom, D. N. Reinhoudt, *Angew. Chem. Int. Ed. Engl.* **35**, 1215 (1996); S. Mann, *Biomimetic Materials Chemistry* (VCH, New York, 1996); A. Firouzi *et al.*, *Science* **267**, 1138 (1995); S. C. Zimmerman, F. Zeng, D. E. C. Reichert, S. V. Kolotuchin, *ibid.* **271**, 1095 (1996); C. T. Kresge, M. E. Leonowicz, W. J. Roth, J. C. Vartuli, J. S. Beck, *Nature* **359**, 710 (1992).
2. N. Khazanovich, J. R. Granja, D. E. McRee, R. A. Milligan, M. R. Ghadiri, *J. Am. Chem. Soc.* **116**, 6011 (1994).
3. H. Huang, E. E. Remsen, K. L. Wooley, *Chem. Commun.* **1998**, 1415 (1998); R. S. Meissner, J. Rebek Jr., J. de Mendoza, *Science* **270**, 1485 (1995); S. A. Jenekhe and X. L. Chen, *ibid.* **279**, 1903 (1998); K. D. Shimizu and J. Rebek Jr., *Proc. Natl. Acad. Sci. U.S.A.* **92**, 12403 (1995).
4. S. Casjens, in *Virus Structure and Assembly*, S. Casjens, Ed. (Jones & Bartlett, Boston, 1995), pp. 75–147; J. M. Grimes *et al.*, *Nature* **395**, 470 (1998).
5. S. N. Timascheff, in *Physical Aspects of Protein Interactions*, N. Catsimpoolas, Ed. (Elsevier-North Holland, Amsterdam, 1978), pp. 219–273.
6. L. R. MacGillivray and J. L. Atwood, *Nature* **389**, 469 (1997); T. Douglas and M. Young, *ibid.* **393**, 152 (1998); V. Percec *et al.*, *ibid.* **391**, 161 (1998); V. S. K. Balagurusamy, G. Ungar, V. Percec, G. Johansson, *J. Am. Chem. Soc.* **119**, 1539 (1997).
7. J. L. Atwood, A. W. Coleman, H. Zhang, S. G. Bott, *J. Inclusion Phenom.* **5**, 203 (1989).
8. C. Tanford, *The Hydrophobic Effect* (Wiley, New York, 1973).
9. G. M. Whitesides, J. P. Mathias, C. T. Seto, *Science* **254**, 1312 (1991); A. Terfort, N. Bowden, G. M. Whitesides, *Nature* **386**, 162 (1997).
10. J. L. Atwood *et al.*, *J. Am. Chem. Soc.* **113**, 2760 (1991); J. L. Atwood *et al.*, *Inorg. Chem.* **31**, 603 (1992).
11. The spherical assembly crystallizes in the trigonal system, space group *R*3 (number 148), unit cell edges $a = b = 44.553(4)$ Å and $c = 35.223(4)$ Å, cell volume $V = 60549(10)$ Å^3, formula units per cell $Z = 18$, calculated density $\rho_{calc} = 1.300$ g cm^{-3}, reliability index $R_1 = 0.132$ [intensity $I > 2\sigma(I)$], and spectral line λ(Mo Kα) = 0.70930 Å; standard errors in the last decimal place are given in parentheses. Details of the x-ray structure determination are available from the Cambridge Crystallographic Data Centre (CCDC) (deposition number CCDC 127797).
12. J. N. Israelachvili, *Intermolecular and Surface Forces* (Academic Press, London, 1985).
13. L. J. Barbour, G. W. Orr, J. L. Atwood, *Nature* **393**, 671 (1998).
14. We sought to control the dimensions of the spherical assemblies (and thus to control the contents of the polar core) by adding varying concentrations of small, aromatic amphiphilic molecules to the three-compo-

nent mixture. These amphiphilic molecules, through a combination of hydrophobic effects and π-stacking interactions, might intercalate into the organic shell of **3** and thereby expand its dimensions as similar effects have been observed in both natural and abiotic systems. For example, the morphology of lecithin vesicles can be modified by incorporating cholesterol molecules into the hydrophobic regions of the membrane interface (*17*). Amphiphilic molecules that were evaluated include the Na salts of benzenesulfonic acid, benzoic acid, and phenol. Success was not met in these cases, and this outcome was attributed to the interference of these compounds with the coordination of **2** to the lanthanide ions.

15. The tubular assembly crystallizes in the trigonal system, space group $P3_112$ (number 151), $a = b = 30.4533(11)$ Å and $c = 16.2800(8)$ Å, $V = 13075.4(9)$ Å^3, $Z = 3$, $\rho_{\mathrm{calc}} = 1.733$ g cm^{-3}, $R_1 = 0.105$ [$I > 2\sigma(I)$], and λ(Mo Kα) = 0.70930 Å; standard errors in the last decimal place are given in parentheses. Details of the x-ray structure determination are available from the CCDC (deposition number CCDC 127798).
16. C. A. Hunter and J. K. M. Sanders, *J. Am. Chem. Soc.* **112**, 5525 (1990).
17. M. N. Jones and C. Chapman, *Micelles, Monolayers, and Biomembranes* (Wiley-Liss, New York, 1995).

18. We thank C. Barnes for crystallographic assistance. This work was supported by the NSF.

16 April 1999; accepted 29 June 1999

Hafnium Isotope Stratigraphy of Ferromanganese Crusts

Der-Chuen Lee,[1] Alex N. Halliday,[2] James R. Hein,[3]
Kevin W. Burton,[4] John N. Christensen,[1] Detlef Günther[5]

A Cenozoic record of hafnium isotopic compositions of central Pacific deep water has been obtained from two ferromanganese crusts. The crusts are separated by more than 3000 kilometers but display similar secular variations. Significant fluctuations in hafnium isotopic composition occurred in the Eocene and Oligocene, possibly related to direct advection from the Indian and Atlantic oceans. Hafnium isotopic compositions have remained approximately uniform for the past 20 million years, probably reflecting increased isolation of the central Pacific. The mechanisms responsible for the increase in ^{87}Sr/^{86}Sr in seawater through the Cenozoic apparently had no effect on central Pacific deep-water hafnium.

Variations in the radiogenic isotope composition of seawater through time have the potential to provide information on changes in continental weathering, ocean floor hydrothermal activity, and ocean circulation (*1–3*) and their relation to tectonic and climatic events (*4–6*). Isotopic records of Sr, Nd, and Pb in ferromanganese crusts from all the major ocean basins have been used to study secular variations of seawater (*7–13*). Because of analytical difficulties, Hf isotopes have received little attention until recently (*14*). Here, we present the first high-resolution and precise Hf isotopic profiles for two ferromanganese crusts dredged from central Pacific seamounts in an attempt to constrain the evolution of Hf isotopes in central Pacific deep water.

The Hf isotopic composition of seawater has yet to be measured directly but might be expected to be far more variable than that of Nd for the following reasons. First, the magnitude of Hf isotopic variations that result from the time-integrated effects of mantle melting and igneous processes is about twice that of Nd (*15*). Second, during weathering, Lu/Hf and Hf isotopic compositions display extreme variability because of selective retention of unradiogenic Hf in the resistant mineral zircon, which tends to be concentrated in coarse coastal and fluvial sands (*16*). This contrasts with the lack of erosional and sedimentary fractionation in the Sm-Nd system (*2*). Third, radiogenic Hf appears to enter seawater through ocean hydrothermal systems (*14, 17*), in contrast to the efficient scavenging of rare earth elements around vents (*18*).

The outermost surfaces of ferromanganese nodules (*19*) and crusts (*14*) have geographically heterogeneous Hf isotopic compositions, suggesting a residence time in seawater that is shorter than the turnover time of the deep oceans. The Hf isotopic composition of crusts from the Pacific is relatively radiogenic compared to those from the Atlantic (*14, 19*), consistent with the ages of the surrounding continental areas (*14, 19*). However, these oceanic variations in Hf are no greater than those found for Nd, which (given the significant isotopic variations in input) implies that the residence time for Hf is probably longer than that of Nd. A major change in the relative importance of a particular flux should therefore produce a change in the regional Hf isotopic composition of seawater, but Hf may be fairly homogeneous within an area such as the Pacific Ocean.

We analyzed two ferromanganese crusts, CD29-2 and D11-1, dredged from central Pacific seamounts at water depths of 2.3 and 1.8 km, respectively (*20*). Both crusts grew throughout most of the Cenozoic and have been studied intensively (*10–12, 20, 21*), and their growth history and state of preservation are well understood. We sliced ~0.5 mm samples through the crusts, each equivalent to a growth interval of about 0.3 million years (My), based on ^{10}Be chronology and extrapolation (*11*). A series of samples with average age differences of ≤ 1 My were analyzed (*22*).

Both crusts exhibit variations in Hf isotopic composition of about $4\varepsilon_{\mathrm{Hf}}$ (*22*) (Fig. 1) and have present-day Hf isotopic compositions that are comparable to those of other hydrogenous crusts from the Pacific (*14, 19*). The two crusts display similar systematic fluctuations in their Hf records from the earliest Eocene until about 20 million years ago (Ma). The $\varepsilon_{\mathrm{Hf}}$ is especially high in both crusts at 25 to 24 Ma and at 33 to 32 Ma and is low at ~28 Ma. The slight offset in these changes between the crusts can be accounted for by the uncertainty of the extrapolated Co and ^{10}Be ages (Fig. 1) (*21*). The more extensive record for D11-1 shows a major dip and rise in the Eocene, and low values at about 44 and 40 Ma. Both crusts display a slight rise in $\varepsilon_{\mathrm{Hf}}$ between 20 and 6 Ma, but the effect is small (Fig. 1).

Phosphatization is a common feature among thick ferromanganese crusts from the Pacific (*23*), and both CD29-2 and D11-1 show evidence of phosphatization before 26 Ma and before 20 Ma, respectively (*11, 23*). However, P concentrations vary by an order of magnitude through the phosphatized interval of each crust (*11, 23*). There is no sign in either crust that the Hf isotopic composition or the Lu/Hf ratio varies with P (Fig. 1). Furthermore, despite very different phosphatization records, the major fluctuations in Hf isotopic composition for the two crusts are well correlated. As a consequence, phosphatization has clearly been of negligible importance to the Hf isotope compositions. Diagenesis is also unlikely to alter the long-term Hf isotope records in ferromanganese crusts (*24*).

Instead, we consider that the Hf isotopic variations reflect gradual modification of central Pacific deep water by changes in sources and circulation through time. That these two crusts, separated by more than 3000 km, yield comparable isotopic compositions indicates that the ambient seawater, central Pacific deep water, has always remained

---

[1]Department of Geological Sciences, University of Michigan, Ann Arbor, MI 48109, USA. [2]Institut für Isotopengeologie und Mineralische Rohstoffe, Department für Erdwissenschaften, ETH-Zentrum, NO C61, Sonneggstrasse 5, CH-8092 Zürich, Switzerland. [3]U.S. Geological Survey, MS 999, 345 Middlefield Road, Menlo Park, CA 94025, USA. [4]Department des Sciences de la Terre, Universite Blaise-Pascal, 63038 Clermont-Ferrand, France. [5]Institut für Analytische Chemie und Spurenanalytik, ETH Zürich, Laboratorium für Anorganische Chemie, Universitätsstrasse 6, CH-8092 Zürich, Switzerland.